HHS Public Access

Author manuscript

Langmuir. Author manuscript; available in PMC 2018 June 01.

Published in final edited form as:

Langmuir. 2018 January 30; 34(4): 1457–1465. doi:10.1021/acs.langmuir.7b02801.

Study of poly (*N*-isopropylacrilamide-*co*-acrylic acid) (pNIPAM) microgel particle induced deformations of tissue mimicking phantom by ultrasound stimulation

Aditya Joshi[1], **Seema Nandi**[2,3], **Daniel Chester**[2,3], **Ashley C. Brown**[*,2,3], and **Marie Muller**[*,1,2]

[1]Department of Mechanical and Aerospace Engineering, North Carolina State University

[2]Joint Department of Biomedical Engineering, North Carolina State University and University of North Carolina at Chapel Hill, Raleigh, NC

[3]Comparative Medicine Institute, North Carolina State University

Abstract

Poly (N-isopropylacrilamide) (pNIPAm) microgels (microgels) are colloidal particles that have been used extensively for biomedical applications. Typically, these particles are synthesized in the presence of an exogenous cross-linker, such as N, N′-Methylenebis (acrylamide) (BIS); however, recent studies have demonstrated that pNIPAm microgels can be synthesized in the absence of an exogenous crosslinker, resulting in the formation of ultra-low crosslinked (ULC) particles, which are highly deformable. Microgel deformability has been linked in certain cases to enhanced bioactivity when ULC microgels are used for the creation of biomimetic particles. We hypothesized that ultrasound stimulation of microgels would enhance particle deformation and that the degree of enhancement would negatively correlate with the degree of particle crosslinking. Here, we demonstrate in tissue-mimicking phantoms that using ultrasound insonification causes deformations of ULC microgel particles. Furthermore, the amount of deformation depends on the ultrasound excitation frequency and amplitude, and on the concentration of ULC microgel particles. We observed that the amplitude of deformation increases with increasing ULC microgel particle concentration up to 2.5 mg / 100 ml, but concentrations higher than 2.5 mg / 100 ml result in reduced amount of deformation. In addition, we observed that the amplitude of deformation was significantly higher at 1 MHz insonification frequency. We also report that increasing the degree of microgel crosslinking reduces the magnitude of the deformation and increases the optimal concentration required to achieve the largest amount of deformation. Stimulated ULC microgel particle deformation has numerous potential biomedical applications, including enhancement of localized drug delivery and biomimetic activity. These results demonstrate the potential of ultrasound stimulation for such applications.

Graphical Abstract

[*]Corresponding Authors: Marie Muller, PhD, Address: Department of Mechanical and Aerospace Engineering, North Carolina State University, 911 Oval Drive, Raleigh, NC 27606, Phone: (919) 515-1186, mmuller2@ncsu.edu. Ashley C. Brown, PhD, Address: Joint Department of Biomedical Engineering, North Carolina State University and University of North Carolina at Chapel Hill, 911 Oval Drive, Raleigh, NC 27606, Phone: (919) 513-8231, aecarso2@ncsu.edu.

Author Contributions

The manuscript was written through contributions of all authors. All authors have given approval to the final version of the manuscript.

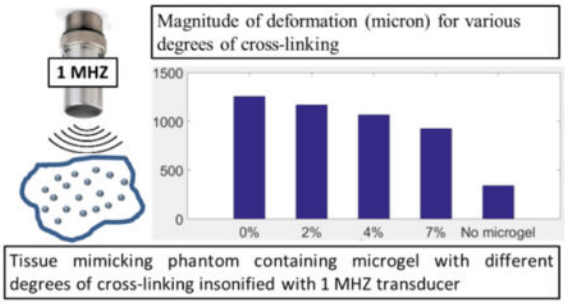

Keywords

microgels; ultrasound; pNIPAM; ultralow crosslinked microgels (ULCs); biomedical

INTRODUCTION

Poly(N-isopropylacrilamide)(pNIPAm) microgels are water-swollen colloid particles that have been utilized for a wide range of biomedical applications including targeted drug delivery and development of hemostatic agents[1]. PNIPAm microgels are synthesized in the presence of an exogenous cross-linker, such as N,N′-Methylenebis(acrylamide) (BIS); however, recent studies have demonstrated that pNIPAm microgels can be synthesized in the absence of an exogenous crosslinker, resulting in the formation of ultra-low cross-linked (ULC) particles[1–4]. Microgel mechanics are easily modulated through alterations in the degree of intra-particle crosslinking. In particular, recent reports have demonstrated that microgel deformability can be modulated through crosslinking[5]. Interestingly, for many biomedical applications, particle deformability directly influences bio-functionality. For example, recent studies developing platelet-like-particles from fibrin-binding ULC microgels demonstrate that a high degree of particle deformability allows these particles to closely mimic natural platelet morphology and shape change following activation[6]. Additionally, this high degree of particle deformability, when coupled with high fibrin affinity, allows the fibrin-binding ULC microgels to spread extensively within and ultimately collapse the fibrin network, a behavior that mimics clot retraction of natural platelets. These biomimetic behaviors are not captured in more highly crosslinked particles. Particle crosslinking and deformability have also been shown to influence drug uptake and release kinetics; higher degrees of microgel crosslinking decrease drug update and release rates[7]. Enhancing particle deformation may further enhance bio-functionality. Indeed, recent reports have demonstrated that application of laser-generated focused ultrasound to microgels can enhance drug release kinetics[8,9]. While the effect of ultrasound of microgel deformability has not been studied previously, interactions between ultrasound and highly deformable droplets and microbubbles have been studied in the last few decades for diagnostic and therapeutic applications[10]. Ultrasound contrast agent (UCA) microbubbles are used in combination with ultrasound insonification for numerous applications, including contrast-enhanced ultrasound imaging[11,12], enhancing effectiveness of High Intensity Focused Ultrasound (HIFU) treatments[13], multiple scattering based quantitative ultrasound tissue characterization[14], targeted drug delivery[15], enhancing drug uptake by tumors[16], and

non-invasive molecular imaging[17]. Advanced technologies such as advanced droplet vaporization (ADV) allow for the use of liquid-based agents rather than gas bubbles that phase-transition into gas bubbles upon insonification with ultrasound. These technologies open up new diagnostic and therapeutic applications based on ultrasound-droplet interactions, such as embolotherapy[18], aberration correction[19], drug delivery[20,21] etc. In these studies, we investigate the effect of ultrasound application to pNIPAm microgels on increasing microgel deformation. Due to the high deformability of microgel particles, we hypothesize that ultrasound pulses can stimulate the enhanced deformation of pNIPAm microgels. In order to study the effect of ultrasound stimulation on microgel particles, we conducted *in vitro* experiments in a tissue-mimicking phantom using a range of microgel concentrations comprised of varying degrees of crosslinking. Because microgel crosslinking has been shown to negatively correlate with particle deformability, we also expected that the degree of deformation upon ultrasound application would increase with decreasing particle crosslinking. Collectively, the results from these studies show the potential of ultrasound stimulation of pNIPAm microgels, and will inform the selection of suitable stimulation frequencies, particle crosslinking and microgel concentrations in future studies that aim at maximizing microgel deformation.

MATERIALS AND METHODS

Microgel synthesis

Poly (*N*-isopropylacrilamide-*co*-acrylic acid) (pNIPAM) microgels were synthesized via a precipitation polymerization reaction. NIPAM (Sigma-Aldrich, St. Louis, MO, USA) was recrystallized in hexanes prior to use. NIPAM (Sigma-Aldrich, St. Louis, MO, USA), acrylic acid (Sigma-Aldrich, St. Louis, MO, USA) and N, N-dimethylenebisacrylamide (BIS) (Sigma-Aldrich, St. Louis, MO, USA) (for crosslinked particles) were dissolved in DI water at a concentration of 10% acrylic acid and 140 mM total monomer. 10% acrylic acid was incorporated into the microgels in order to provide a functional handle for future coupling of desired binding or targeting motifs to the microgels for use in therapeutic applications. Microgels containing varying degrees of crosslinking were created by incorporating 0%, 2%, 4%, or 7% N, N-dimethylenebisacrylamide (BIS) (Sigma-Aldrich, St. Louis, MO, USA) into the precipitation polymerization reaction. Microgels containing 0% BIS are referred to as ultra-low crosslinked microgels (ULCs). The solution was filtered through a 0.2 um pore filter and added to a 3-neck round-bottom flask. An oil bath was heated to 70°C, and then the round-bottom flask was added into the bath, stirred at 450 rpm, and purged with nitrogen. After equilibrating at 70°C for an hour, the reaction was initiated using ammonium persulfate (APS) (Sigma-Aldrich, St. Louis, MO, USA) and carried out for 5.5 hours at a constant temperature of 70 °C and a stir speed of 450 rpm. In all cases, the synthesis turned distinctly opaque, indicating successful polymer formation. Mass fraction measurements of colloidal microgels vs. aggregates were determined immediately after synthesis by collecting aggregates in a glass wool filtration step and weighing both colloidal microgels and aggregates. After mass fraction was determined, aggregates were discarded and only colloidal microgels were purified and subsequently studied. Microgels were dialyzed (MWCO: 1000 kD from Spectrum Labs, Rancho Dominguez, CA, USA) for three days following synthesis against ultrapure diH_20 and were then lyophilized and resuspended in

ultrapure diH_20. Microgel size was characterized using a Malvern Zetasizer Nano S to perform dynamic light scattering (DLS) and using a Malvern Nanosight NS300 on microgels suspended in 10 mM formate buffer (pH 3.0). Microgel spreading on a glass surface was analyzed using an Asylum Research MFP-3D Bio atomic force microscope (AFM). Microgels were deposited onto clean glass slides and imaged in air using silicon nitride cantilevers (k=42 N m1, NanoWorld) operated in intermittent contact mode. Microgel morphology was characterized using a JEOL 7600F cryogenic scanning electron microscope with a Gatan Alto Cryo-transfer system. Microgel samples suspended in ultrapure water were plunge-frozen in liquid nitrogen, fractured, and etched for five minutes prior to gold sputter-coating and imaging.

Preparation of tissue mimicking phantom

Various tissue mimicking phantoms have been proposed for studying ultrasound propagation in the past few decades[22–27]. Ideal ultrasound phantoms should match the speed of sound, density and attenuation of soft tissue. We prepared the phantom following the procedure proposed by Dunmire et al[28]. These phantoms were prepared from agar-gelatin gel combined with aluminum oxide particles. To make the phantom, 4 mg 80-mesh aluminum oxide powder (Sigma-Aldrich, St. Louis, MO, USA) was added to 4 ml propanol (Fisher Scientific, Hampton, NH, USA), and 0.2 mg potassium sorbate (LD Carlson Company, Kent, OH, USA) was added to 200 ml degassed water. Potassium sorbate acts as a preservative. The speed of sound in the phantom can be altered by varying the amounts of gelatin and propanol. The microgel particles do not have a significant impedance contrast with water. Hence, they are undetectable by ultrasound imaging. Thus, in order to track deformations within the phantoms, aluminum oxide particles were added to the agar-gelatin gel to provide speckle in ultrasound images. The speckle will be used to track deformations within the phantom. After degassing both these mixtures in a vacuum chamber for 1 hour, they were mixed together and then heated at a rate of about 1 °C per minute using a hotplate with a magnetic stirrer (VWR International, Radnor, PA, USA). 8 mg of gelatin powder derived from porcine skin (Sigma-Aldrich, St. Louis, MO, USA) was then added gradually (to avoid formation of lumps) to this mixture, maintaining constant stirring, until the gelatin was completely dissolved in water. 4 mg of agar powder (Fisher scientific, Hampton, NH, USA) was then gradually added to this mixture. The temperature of the mixture was maintained at 90°C, above the melting point for gelatin (which is 35°C) and agar (which is 85°C). Once agar was completely dissolved in the mixture, the heat was turned off and the mixture was allowed to cool to 40°C under constant stirring. Microgel particles with varying degrees of crosslinking were added to these mixtures in varying concentrations, and the mixture was further allowed to cool to room temperature under constant stirring. The solidification temperature for agar is around 35 °C [29]. This difference between solidification temperature and melting point is due to hysteresis effect; thus, the mixture is still homogeneous at 40 °C The pH of the mixture was 7.4 ± 0.05, which is equal to biological pH. The concentration of microgel particles was varied from 0.5mg / 100 ml of water to 4 mg / 100 ml of water in steps of 0.5 mg / 100 ml of water. A control phantom was prepared without any microgel particles, which acted as datum for deformation measurements. At this stage, the jar containing the gel was placed in a refrigerator overnight prior to testing. Samples in which settling of aluminum oxide particles was observable in ultrasound images

were discarded. Aluminum oxide particles settled in very few cases (a total of five samples were discarded while acquiring the entire dataset collected for this experiment), because the temperature of the sample could not be precisely monitored after addition of microgel particles at 40 °C (the thermocouple had to be removed before jellification started). The stirring magnet was removed shortly after addition of microgel particles to stop stirring and the sample was refrigerated immediately. Because the cooling rate was a function of ambient conditions (temperature, pressure, RH etc.) that were not monitored, aluminum oxide particles settled in the few samples for which the cooling rate was insufficient.

The colloidal behavior of aluminum oxide particles in the presence of organic matter is dependent on the pH of the solution. At an alkaline pH, the colloid is stable. As the tissue mimicking phantom had a pH of 7.4, no interaction between the aluminum oxide particle and the microgels is expected[30]. To ensure the repeatability of the results, three samples were prepared for each concentration.

Experimental setup and data acquisition

Two types of ultrasound insonification were implemented simultaneously, in order to both stimulate and image the phantoms. For stimulation, we used single element plane immersion transducers with various central frequencies, ranging from 0.5 MHz to 4 MHz (Olympus Corporation, PA, USA). The stimulation signal was a continuous sine wave pulse with 2 MPa peak-to-peak pressure generated using a Keysight arbitrary waveform function generator (Keysight Technologies, Santa Rosa, CA, USA). The pressure was calibrated using a hydrophone (Ondo Corp., Sunnyvale, CA, USA). For imaging, we used a L11-4v linear array transducer connected to a Vantage 128 research platform (Verasonics, Redmond, WA, USA) operating at 7.8 MHz. Because the ultrasound stimulation was in the MHz range, high frame rate imaging was required, and was achieved using plane wave imaging instead of conventional ultrasound B-mode imaging. Plane waves were transmitted using the array, and we used parallel receive beamforming to achieve the frame rates[31]. The frame rate was 9995 images/second. The field of view was 38.4 mm (lateral) by 40 mm (in depth). This technique is commonly used for shear wave Elastography, ultrafast contrast imaging, and functional ultrasound imaging of brain activity[31–33]. Both the linear array transducer (used for plane wave imaging) and the single element transducer (used for stimulation) were synchronously triggered using LabVIEW NI-DAQmx (National Instruments, Austin, TX, USA) with a precision of 50 ns ± 5 ns. The Verasonics scanner was used to trigger the data acquisition. However, even with such high frame rates, because the ultrasound stimulation is in the MHz range, it is impossible to track the motion of the particles in real time. Stroboscopic imaging was therefore required to track the motion of the scatterers (the aluminum oxide particles). A schematic diagram showing the experimental setup is shown in Figure 1. The imaging sequence was repeated over 6 angles ranging between −25 °C to 25°C in steps of 10°C to reconstruct the image using the coherent compounding[34], in order to improve the lateral resolution of the acquired plane wave images.

By acquiring the images at a precisely controlled 9.995 kHz frequency, i.e. 1 frame per 100.05 μs, we can effectively get multiple points per period of stimulation wavelength. For example, for 1 MHz stimulation, (period 1 μs) by acquiring 1 point after every 100 cycles,

each time advancing by 0.05 μs we can track one full stimulation cycle is after 2001 actual stimulation cycles. In other words, we acquire 20 points per period of stimulation cycle, although any two points are actually 100 cycles apart. This idea is illustrated in Figure 2. Due to limited precision of the Verasonics trigger (50 ns ± 5 ns); acquisition frequency was kept constant at 9.995 kHz. Thus, the number of points per period of stimulation cycle varied from five at 4 MHz to forty at 0.5 MHz.

Total acquisition time was 20 ms, for every angle, which enabled capturing at least 10 stimulation cycles for all stimulation frequencies. The total acquisition time for one complete set of readings for one sample was less than 10 seconds.

Displacement tracking and image processing

Displacements within the phantom due to stimulation were measured using the algorithm proposed by Niu et al[35]. This method is a modified version of the PIV (particle image velocimetry) algorithm[36] with several modifications including an iterative approach, a subpixel method, filtering and interpolation methods, and spurious vector elimination algorithm implemented using an universal outlier detection method as described by Westerweel et al.[37] to improve accuracy of the measurements. The detailed procedure for data acquisition and image processing is shown in Figure 3. The first step after acquisition is the coherent compounding of the images acquired along different angles to improve lateral resolution. In incoherent compounding, several frames are summed to cancel out random variations (noise), whereas coherent compounding consists of coherent summation of ultrafast images obtained from plane wave transmissions at different angles[34]. Montaldo et al.[34] demonstrated that coherent plane-wave compounding could produce image quality equivalent to image quality of the optimal multifocus images.

To obtain a displacement map, two consecutive ultrasound images of region of interest (80 ×120 wavelengths) were divided into several regions of interest each. For each window, cross-correlation analysis between two consecutive images was performed to compute a local displacement using the algorithm proposed by Niu et al.[35]. The displacement in each position was then fitted with a sine curve, and the mean amplitude of the sine wave was reported as the deformation produced.

Drug loading and release

ULCs and 7% BIS microgels were loaded with 20 kDa dextran (VWR International, Radnor, PA, USA) labeled with fluorescein isothiocyanate (Fisher Scientific, Hampton, NH, USA) by swelling 10 mg of each microgel type in 500 μL of dextran solution (2.25 mg/ml dextran in 10 mM HEPES buffer, pH 7.4) for 24 hours. Microgel suspensions were spun in a microcentrifuge at 21.1 × g for 15 minutes. The supernatants were collected and the pellets were resuspended in 500 μL 10 mM HEPES, pH 7.4. Samples were centrifuged and supernatants were collected every hour for the first 6 hours and then at 12 and 24 hours. Samples exposed to ultrasound were transferred to a 12-well plate between collection time points (VWR International, Radnor, PA, USA) and kept in contact with a transducer applying ultrasound at a frequency of 1 MHz for 10 μs in cycles of 250 μs. Fluorescent readings from the supernatants collected at each time point were obtained using a plate

reader. A standard curve was created using solutions of FITC-labeled dextran in 10 mM HEPES buffer. Cumulative drug release over 24 hours was calculated from the obtained fluorescence readings.

Statistical Analysis

Statistical analysis was performed using Prism (Graphpad). Data was analyzed using a One-way ANOVA with a Tukey's posthoc test. Statistical significance is defined as a minimum of $p<0.05$.

RESULTS

Microgel Characterization

Mass fraction of aggregate vs. colloidal microgels was measured post-synthesis and was found to be 94% colloidal microgels and 6% aggregate. Microgels were characterized using dynamic light scattering (DLS), cryogenic scanning electron microscopy (cryoSEM) and atomic force microscopy (AFM) in order to determine their size and deformability. Size measurements were obtained using DLS on microgel suspensions in 10 mM formate buffer, pH 3.0 (Table 1). Particle size distribution was also evaluated using nanoparticle tracking analysis on a Malvern Nanosight NS300 (Figure S1). All particles displayed Gaussian size distributions. Sizes were determined to be 624 ± 32 nm, 754 ± 79 nm, 687 ± 57 nm, and 615 ± 74 nm for ULCs, 2%, 4%, and 7% BIS particles respectively using Nanosight analysis. These average sizes are slightly smaller than the sizes obtained using DLS, however, these differences are to be expected due to the difference in particle measurement techniques between the two instruments. Deformability was then characterized by the ability of the particles to spread on a glass surface (characterized by AFM imaging) and by their morphology visualized by cryoSEM.

Height traces and spread areas were obtained from AFM analysis of microgels deposited on glass coverslips; microgel volume was calculated from spread area and height traces assuming a cylindrical geometry of microgels deposited on glass coverslips. Differences in height traces and microgel volume obtained via AFM analysis revealed differences in microgel deformability (Figure 4). ULC microgels (i.e. 0% BIS) show the highest extent of deformability, as seen by the decreased height and volume of ULC particles on a glass surface relative to crosslinked microgels on a glass surface. Furthermore, greater degrees of crosslinking are shown to decrease microgel deformability, as seen by the greater height and volume exhibited by the 7% BIS microgels relative to the 2% and 4% BIS microgels. Specifically, microgel heights were found to be 24.8 nm ± 14.0 nm for the ULCs, 78.7 nm ± 12.7 nm for the 2% BIS microgels, 90.5 nm ± 12.0 nm for the 4% BIS microgels, and 116.8 nm ± 12.1 nm for the 7% BIS microgels. All crosslinked microgel heights were found to be significantly different from ULC heights, as well as from each other. Microgel volumes were found to be 0.022 ± 0.01 um^3 for the ULCs, 0.032 ± 0.008 um^3 for the 2% BIS microgels, 0.083 ± 0.027 um^3 for the 4% BIS microgels, and 0.084 ± 0.052 um^3 for the 7% BIS microgels.

CryoSEM was additionally used to characterize microgel morphology in suspension. Microgels with greater degrees of crosslinking exhibit lower particle-particle interactions and less deformation than both ULCs and microgels with lower degrees of crosslinking (Figure 5); this corroborates the lower degree of deformability observed via AFM.

Microgels containing 1% BIS were also characterized (Figure S2). Although these microgels were a different size than the 0, 2, 4, and 7% BIS microgels used in this study, these 1% BIS particles were found to display low height profiles as characterized by AFM, similar morphology in cryoSEM images as ULC microgels, and high degrees of deformation in response to ultrasound stimulation.

Effect of ultrasound stimulation on microgel deformation

Following characterization of microgel deformability as a function of particle crosslinking, we next studied the effect of ultrasound stimulation on microgel particles in vitro in a tissue-mimicking phantom. We prepared phantoms in the presence of the microgel particles with varying degrees of crosslinking characterized above using microgel concentrations ranging from 0–0.040 mg/ml. Phantoms were subjected to continuous ultrasound stimulation in the form of continuous sine wave insonification of various frequencies ranging between 0.5 MHz and 4 MHz in steps of 0.25 MHz Using high-frame-rate stroboscopic ultrasound imaging, we tracked the deformation of tissue mimicking phantoms by tracking the displacement of aluminum oxide particles, which act as scatterers in the otherwise anechoic tissue mimicking phantom using high-frame-rate stroboscopic imaging. Figure 6 shows results for the entire set of experiments. The magnitude of deformation indicated in the plots is calculated by averaging the values obtained from thirty readings acquired from three phantoms (ten from each phantom) for each given stimulation frequency, microgel concentration, and crosslinking percentage.

As shown in Figure 6(a), the magnitude of the deformation is maximum at 1 MHz frequency for all phantoms containing microgels with 0% cross-linking at all concentrations. Also, an increase in the concentration of microgels in the phantom results in an increase in the magnitude of deformation, up to an optimal concentration of microgels. Beyond this optimal concentration, further increases in microgel concentration will lead to a decrease in magnitude of the deformation. This reduction in magnitude of the deformation could be attributed to a shielding effect caused by increased density of microgel particles. A similar trend is observed in Figure 6(b–d) in case of microgels with 2%, 4% and 7% crosslinking, respectively. The trend is also seen in smaller 1% BIS microgels (Figure S2(e)). We can also observe from Figures 6(a) and (b) that the magnitude of the deformation is maximum at a microgel concentration of 2.5 mg / 100 ml for 0% and 2% crosslinked microgels. For 4% and 7% crosslinked microgels, as observed in Figure 6(c) and 6(d), the magnitude of the deformation is maximum at microgel concentrations of 2 mg / 100 ml and 1.5 mg / 100, respectively. The magnitude of the deformation within the tissue-mimicking phantom in the absence of microgel particles is significantly lower than the magnitude of deformation in the presence of microgel particles in all cases.

The presence of microgel particles enhances the deformation of a tissue-mimicking phantom subjected to ultrasound stimulation. Deformation is maximum for a stimulation frequency

close to 1 MHz. We propose that the increased deformation of the phantom, especially at stimulation frequencies close to 1 MHz, is caused by the resonance of the microgels. When stimulated by ultrasound, microbubbles (similar in size to the microgels) placed in an incompressible medium will resonate at frequencies in the MHz range[38]. By analogy with the microbubble behavior, it could be hypothesized that the increased response of the microgels at 1 MHz might be attributed to a resonance. This is only a hypothesis, and a complete analytical model is planned for future works, which will have to be validated by experimental studies of dynamics of soft gel nanoparticles using a high-speed optical camera. Furthermore, increasing crosslinking within the microgels themselves has an adverse effect on individual particle deformability. This is expected, since, as illustrated via AFM and cryo-SEM, microgels with increased degrees of crosslinking display less individual particle deformability and undergo fewer particle-particle interactions. Figure 7 shows magnitude of the deformation as a function of degree of crosslinking.

We also observed a linear increase in the magnitude of deformation with an increase in excitation amplitude, especially at lower amplitudes. As shown in Figure 8, for the samples containing microgel with 0% cross-linking, under optimal parameters (Concentration of 2.5 mg / 100 ml of water and stimulation frequency of 1 MHz), there is a linear increase in the magnitude of deformation at pressure below 1.5 MPa whereas there is hardly any increase in magnitude of deformation when pressure was increased from 1.5 MPa to 2 MPa. A slightly different behavior was observed in case of the samples containing microgel with 7% cross-linking. A continuous linear increase in deformation amplitude was observed with an increase in pressure amplitude from 0.5 MPa to 2 MPa. Although higher-pressure amplitude could have been tested, such high pressures are out of the range of in-vivo applications.

Effect of ultrasound and crosslinking density on drug loading and release

Following studies of microgel deformation in the presence of ultrasound, we investigated the effect of ultrasound on drug release kinetics from microgels of low (ULC) and high (7% BIS) crosslinking densities. Microgels were loaded with 20 kDa fluorescently-labeled dextran, and the release of the dextran molecules from the microgels was monitored via fluorescence readings over 24 hours. Microgels containing 7% BIS crosslinker did not show significant changes in dextran release in the presence of ultrasound; however, application of ultrasound has a significant effect on dextran release from ULCs (Figure 9), resulting in an ~30% difference in normalized dextran release. Specifically, we observe a decrease in release rates from ULC microgels in the presence of ultrasound. Dextran release from ULCs not subjected to ultrasound was also significantly higher than dextran release from 7% crosslinked microgels in both the presence and absence of ultrasound stimulation. Cumulative release profiles obtained from fluorescence readings of supernatant solutions reveal that application of ultrasound to ULC microgels can be used to tune release kinetics for use in various therapeutic applications. This could be particularly useful in applications where extended release is desired, compared to burst release, or in cases where differential kinetics are desired in one system.

Discussion

Here, we demonstrate in tissue-mimicking phantoms that using ultrasound insonification causes deformations of ULC microgel particles. The amount of deformation depends on the ultrasound excitation frequency and amplitude, and on the concentration of ULC microgel particles.

Additionally, we observe that the application of ultrasound to ULC microgels results in an ~30% change in drug release kinetics, while application of ultrasound to 7% BIS crosslinked microgels has no effect on release kinetics. It is worth noting that the observation of the microgel deformations are indirect. Because the microgels are not detectable on ultrasound images, only the displacements of aluminum oxide particles could be observed. This is a limitation of this study. However, we propose the hypothesis that larger displacements and deformations within the tissue-mimicking phantom are related to mechanical deformations of the individual microgels. This hypothesis is supported by the finding that ultrasound stimulation of phantoms containing no microgels (0 mg / 100 ml) lead to significantly smaller deformations of the tissue-mimicking phantoms. We observed an optimum in the concentration of microgels that lead to greater deformations. This could be interpreted as a shielding effect, in which a too large concentration of microgels would alter ultrasound propagation. The hypothesis that ultrasound stimulation is responsible for the direct deformation (and possibly resonance) of individual microgels will be tested in future work, through the direct observation of microgel deformations under ultrasound stimulation using ultra high frame rate cameras. However, this is out of the scope of the present study.

The ULC microgels seemed to respond better to an ultrasound stimulation around 1 MHz. It is possible that this might be due to a resonance of the microgels. When stimulated by ultrasound, microbubbles (similar in size to the microgels) placed in an incompressible medium will resonate at frequencies in the MHz range. By analogy with the microbubble behavior, it could be hypothesized that the increased response of the microgels at 1 MHz might be attributed to a resonance. This is only a hypothesis, and a complete analytical model is planned for future works along with experimental study of dynamics of soft gel nanoparticles using a high-speed optical camera.

CONCLUSION

The studies presented here indicate pNIPAm microgel particle deformation can also be enhanced using ultrasound stimulation. This opens up the possibility of combining pNIPAm microgel particles with ultrasound in future studies for applications where enhanced deformation of microgels is desired. In particular, this study can be used as a guide for selecting a suitable stimulation frequency for such studies. By controlling the deformations of microgel particles, we except that the functionality of microgels designed for biomedical applications, such as the bio-mimetic particles or drug delivery particles, will be enhanced. The knowledge acquired by studying the effect of the microgel particles concentration and the stimulation frequency on the degree of deformation can be used in future studies to improve bio-functionality of pNIPAm microgels using ultrasound stimulation.

Supplementary Material

Refer to Web version on PubMed Central for supplementary material.

Acknowledgments

Funding Sources

Funding for this project was provided by NIH NIAMS R21AR071017. Part of this work was performed in part at the Analytical Instrumentation Facility (AIF) at North Carolina State University, which is supported by the State of North Carolina and the National Science Foundation (award number ECCS-1542015). The AIF is a member of the North Carolina Research Triangle Nanotechnology Network (RTNN), a site in the National Nanotechnology Coordinated Infrastructure (NNCI).

The authors acknowledge the Analytical Instrumentation Facility at North Carolina State University and Dr. Chuanzhen Zhou for assistance with cryo-SEM.

References

1. Gao J, Frisken BJ. Influence of Secondary Components on the Synthesis of Self-Cross-Linked N-Isopropylacrylamide Microgels. Langmuir. 2005; 21:545–551. [PubMed: 15641822]
2. Gao J, Frisken BJ. Cross-Linker-Free N-Isopropylacrylamide Gel Nanospheres. Langmuir. 2003; 19:5212–5216.
3. Gao J, Frisken BJ. Influence of Reaction Conditions on the Synthesis of Self-Cross-Linked N-Isopropylacrylamide Microgels. Langmuir. 2003; 19:5217–5222.
4. Virtanen OLJ, Mourran A, Pinard PT, Richtering W. Persulfate initiated ultra-low cross-linked poly(N-isopropylacrylamide) microgels possess an unusual inverted crosslinking structure. Soft Matter. 2016; 12:3919–3928. [PubMed: 27033731]
5. Bachman H, Brown AC, Clarke KC, Dhada KS, Douglas A, Hansen CE, Herman ES, Hyatt JS, Kodlekere P, Meng Z, Saxena S, Spears MW Jr, Welsch N, Lyon LA. Ultrasoft, highly deformable microgels. Soft Matter. 2015; 11:2018–2028. [PubMed: 25648590]
6. Brown AC, Stabenfeldt SE, Ahn B, Hannan RT, Dhada KS, Herman ES, Stefanelli V, Guzzetta N, Alexeev A, Lam WA, Lyon LA, Barker TH. Ultrasoft microgels displaying emergent platelet-like behaviours. Nat Mater. 2014; 13:1108–1114. [PubMed: 25194701]
7. Fernandez-Nieves, A., Wyss, HM., Mattsson, J., Weitz, D. A Microgel Suspensions: Fundamentals and Applications. Wiley-VCH Verlag GmbH & Co. KGaA, Wiley; New York: 2011. p. 375-405.
8. Di J, Kim J, Hu Q, Jiang X, Gu Z. Spatiotemporal drug delivery using laser-generated-focused ultrasound system. J Control Release. 2015; 220:592–599. [PubMed: 26299506]
9. Qi X, Xiong L, Peng J, Tang D. Near infrared laser-controlled drug release of thermoresponsive microgel encapsulated with Fe_3O_4 nanoparticles. RSC Adv. 2017; 7:19604–19610.
10. Escoffre, JM., Bouakaz, A. Advances in Experimental Medicine and Biology. Vol. 880. Springer; Berlin: 2016. Therapeutic Ultrasound; p. 157-338.
11. Gramiak R, Shah PM. Echocardiography of the Aortic Root. Invest Radiol. 1968:3.
12. Gessner, RC., Frederick, CB., Foster, FS., Dayton, PA. Acoustic angiography: a new imaging modality for assessing microvasculature architecture. Int J Biomed Imaging [Online]. 2013. https://www.hindawi.com/journals/ijbi/2013/936593/
13. Unger EC, Porter T, Culp W, Labell R, Matsunaga T, Zutshi R. Therapeutic applications of lipid-coated microbubbles. Adv Drug Deliv Rev. 2004; 56:1291–1314. [PubMed: 15109770]
14. Joshi A, Muller M, Shelton S, Papadopoulou V, Lindsey B, Dayton PA. In-vivo quantitative analysis of the angiogenic microvasculature in tumor-bearing rats using multiple scattering: A preliminary study. J Acoust Soc Am. 2016; 140:3187.
15. Karshafian R, Bevan PD, Williams R, Samac S, Burns PN. Sonoporation by ultrasound-activated microbubble contrast agents: effect of acoustic exposure parameters on cell membrane permeability and cell viability. Ultrasound Med Biol. 2009; 35:847–860. [PubMed: 19110370]

16. Unger EC, Hersh E, Vannan M, Matsunaga TO, McCreery T. Local drug and gene delivery through microbubbles. Prog Cardiovasc Dis. 2001:44–54.
17. Lindner JR. Microbubbles in medical imaging: current applications and future directions. Nat Rev Drug Discov. 2004; 3:527–533. [PubMed: 15173842]
18. Zhang M, Fabiilli ML, Haworth KJ, Fowlkes JB, Kripfgans OD, Roberts WW, Ives KA, Carson PL. Initial investigation of acoustic droplet vaporization for occlusion in canine kidney. Ultrasound Med Biol. 2010; 36:1691–1703. [PubMed: 20800939]
19. Carneal CM, Kripfgans OD, Krucker J, Carson PL, Fowlkes JB. A Tissue-Mimicking Ultrasound Test Object Using Droplet Vaporization to Create Point Targets. IEEE Trans Ultrason Ferroelectr Freq Control. 2011; 58:2013–2025. [PubMed: 21937339]
20. Fabiilli ML, Haworth KJ, Sebastian IE, Kripfgans OD, Carson PL, Fowlkes JB. Delivery of Chlorambucil Using an Acoustically-Triggered, Perfluoropentane Emulsion. Ultrasound Med Biol. 2010; 36:1364–1375. [PubMed: 20691925]
21. Fabiilli ML, Lee JA, Kripfgans OD, Carson PL, Fowlkes JB. Delivery of water-soluble drugs using acoustically triggered perfluorocarbon double emulsions. Pharm Res. 2010; 27:2753–2765. [PubMed: 20872050]
22. Madsen EL, Zagzebski JA, Banjavie RA, Jutila RE. Tissue mimicking materials for ultrasound phantoms. Med Phys. 1978; 5:391–394. [PubMed: 713972]
23. Madsen EL, Zagzebski JA, Frank GR. Oil-in-gelatin dispersions for use as ultrasonically tissue-mimicking materials. Ultrasound Med Biol. 1982; 8:277–287. [PubMed: 7101576]
24. Cook JR, Bouchard RR, Emelianov SY. Tissue-mimicking phantoms for photoacoustic and ultrasonic imaging. Biomed Opt Express. 2011; 2:3193–3206. [PubMed: 22076278]
25. Kondo T, Kitatuji M, Kanda H. New tissue mimicking materials for ultrasound phantoms. IEEE Ultrasonics Symposium, 2005. 2005; 3:1664–1667.
26. Madsen EL, Hobson MA, Shi H, Varghese T, Frank GR. Tissue-mimicking agar/gelatin materials for use in heterogeneous elastography phantoms. Phys Med Biol. 2005; 50:5597–5618. [PubMed: 16306655]
27. Ling, T., Jin, Q., Yao, H., Zheng, H. Design and Characterization of a Tissue-Mimicking Phantom for Ultrasonic Elastography. 4th International Conference on Bioinformatics and Biomedical Engineering; 2010. p. 1-4.
28. Dunmire B, Kucewicz JC, Mitchell SB, Crum LA, Sekins KM. Characterizing an Agar/Gelatin Phantom for Image Guided Dosing and Feedback Control of High-Intensity Focused Ultrasound. Ultrasound Med Biol. 2013; 39:300–311. [PubMed: 23245823]
29. McHugh, DJ. Production and utilization of products from commercial seaweeds. Rome: Food and Agriculture Organization of the United Nations; 1987. p. 1-57.
30. Ghosh S, Mashayekhi H, Pan B, Bhowmik P, Xing B. Colloidal behavior of aluminum oxide nanoparticles as affected by pH and natural organic matter. Langmuir. 2008; 24:12385–12391. [PubMed: 18823134]
31. Leow CH, Bazigou E, Eckersley RJ, Yu ACH, Weinberg PD, Tang M. Flow Velocity Mapping Using Contrast Enhanced High-Frame-Rate Plane Wave Ultrasound and Image Tracking: Methods and Initial in Vitro and in Vivo Evaluation. Ultrasound Med Biol. 2017; 41:2913–2925.
32. Gateau J, Aubry JF, Pernot M, Fink M, Tanter M. Combined passive detection and ultrafast active imaging of cavitation events induced by short pulses of high-intensity ultrasound. IEEE Trans Ultrason Ferroelectr Freq Control. 2011; 58:517–532. [PubMed: 21429844]
33. Tanter M, Fink M. Ultrafast imaging in biomedical ultrasound. IEEE Trans Ultrason Ferroelectr Freq Control. 2014; 61:102–119. [PubMed: 24402899]
34. Montaldo G, Tanter M, Bercoff J, Benech N, Fink M. Coherent plane-wave compounding for very high frame rate ultrasonography and transient elastography. IEEE Trans Ultrason Ferroelectr Freq Control. 2009; 56:489–506. [PubMed: 19411209]
35. Niu L, Qian M, Wan K, Yu W, Jin Q, Ling T, Gao S, Zheng H. Ultrasonic particle image velocimetry for improved flow gradient imaging: algorithms, methodology and validation. Phys Med Biol. 2010; 55:2103–2010. [PubMed: 20299721]
36. Adrian RJ. Particle-imaging techniques for experimental fluid mechanics. Annual Review of Fluid Mechanics. 1991; 23:261–304.

37. Westerweel J, Scarano F. Universal outlier detection for PIV data. Exp Fluids. 2005; 39:1096–1100.

38. Sboros V. Response of contrast agents to ultrasound. Adv Drug Deliv Rev. 2008; 60:1117–1136. [PubMed: 18486270]

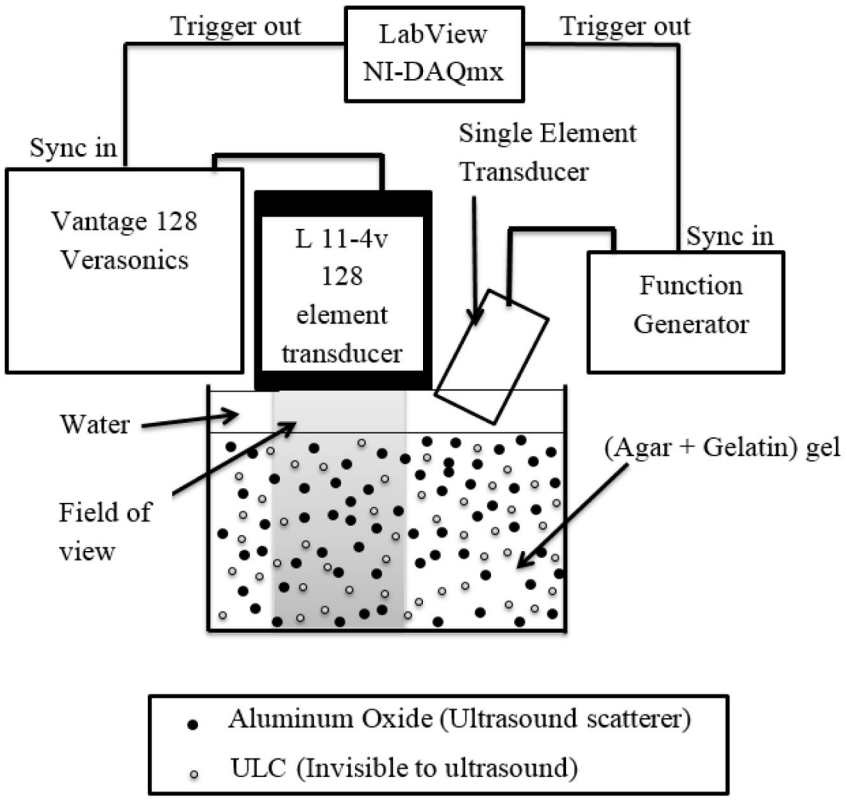

Figure 1.
Experimental setup for high frame rate stroboscopic plane wave imaging of tissue mimicking phantom under ultrasound stimulation

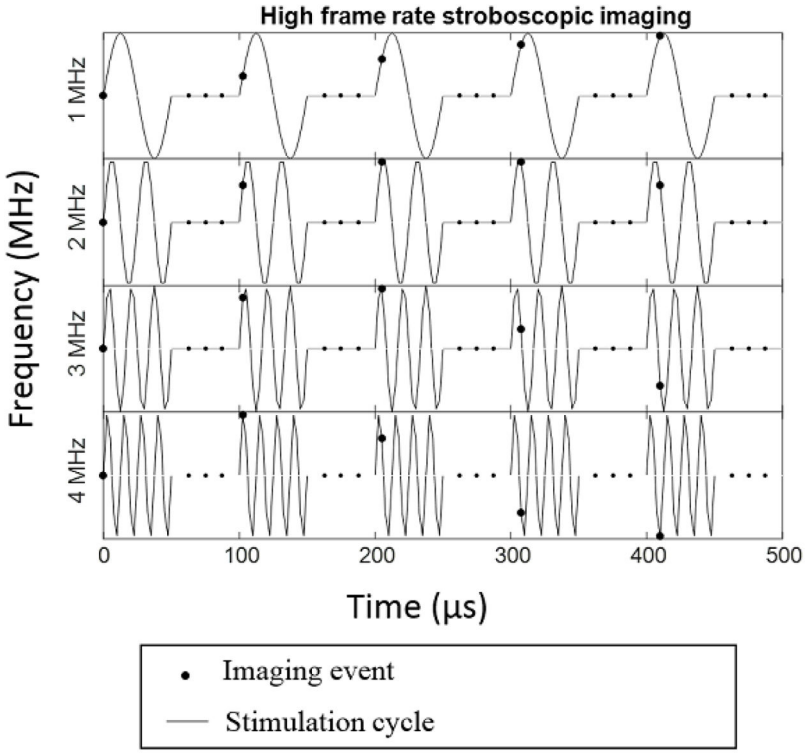

Figure 2.
Schematic diagram of the Stroboscopic imaging of deformation of phantom under ultrasound stimulation.

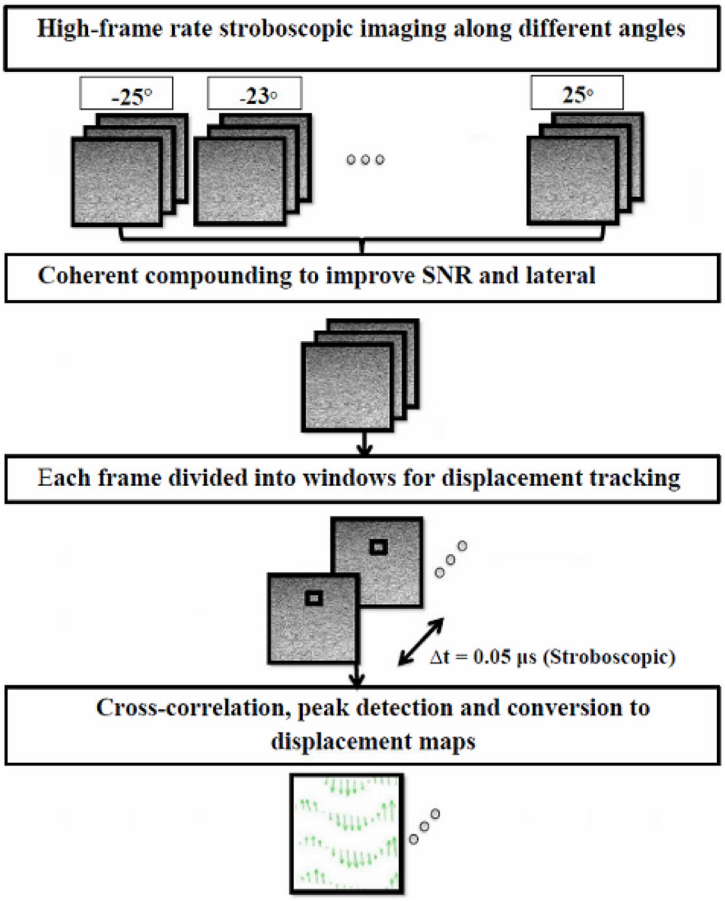

Figure 3.
Steps involved in image processing required to produce displacement maps

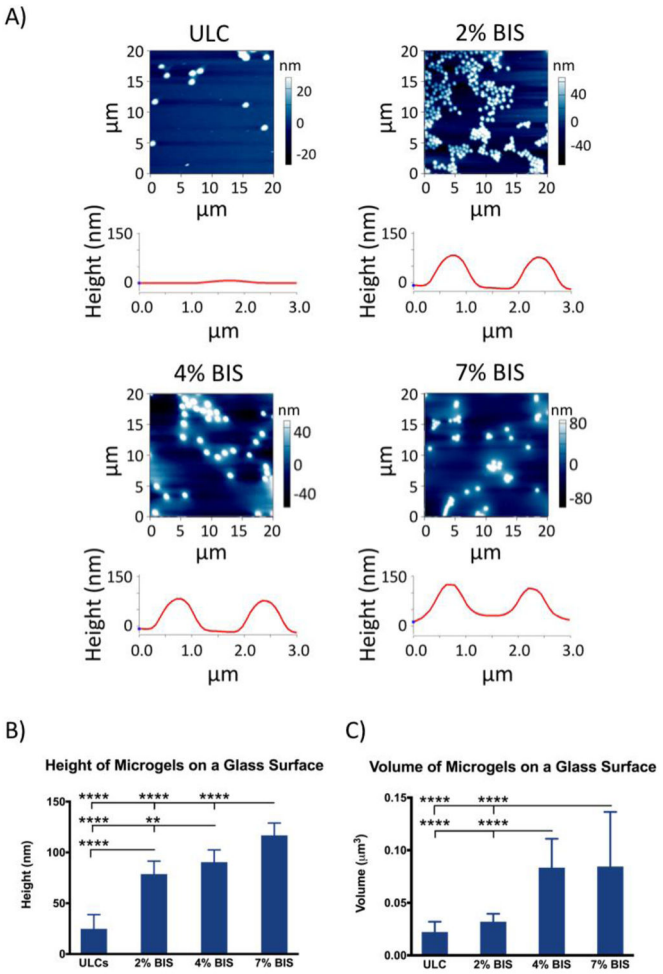

Figure 4.

(a) AFM scans and corresponding representative height traces for each microgel type after deposition on a glass coverslip. (b) Average height of each microgel type after deposition on a glass surface. (c) Average volume of each microgel type, obtained from height and spread areas of each microgel type after deposition on a glass surface. A minimum of 30 particles were analyzed per microgel type. Error bars represent standard deviations from the mean. **: $p < 0.01$; ****: $p < 0.0001$.

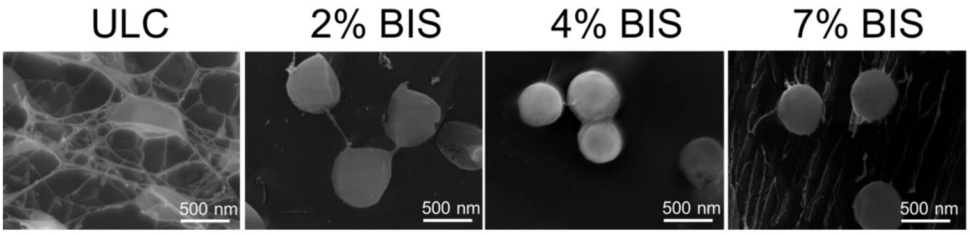

Figure 5.

CryoSEM images of each microgel type taken at 50000X showing microgel morphology in solution. Greater degrees of crosslinker result in less deformable microgels that undergo fewer particle-particle interactions than the microgels containing lower percentages of crosslinker.

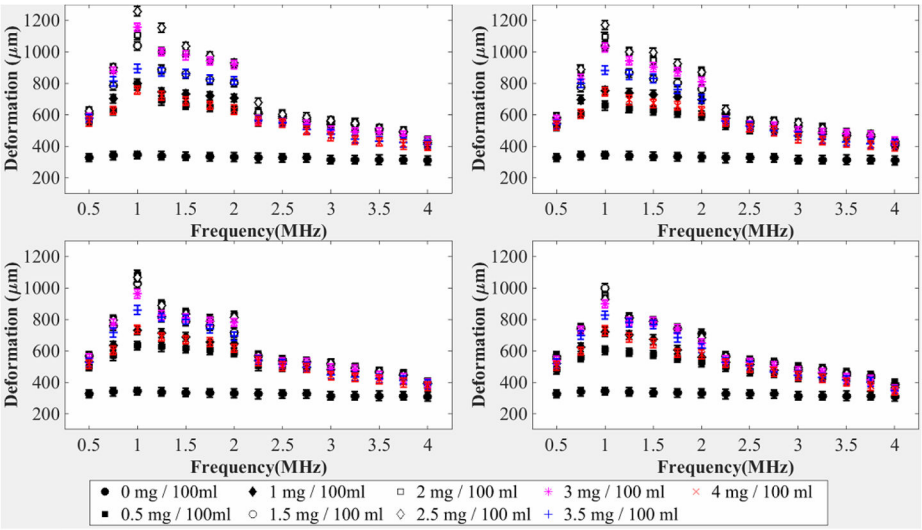

Figure 6.

(a) Deformation of the tissue-mimicking phantom (microns) containing microgels with 0% cross-linking versus stimulation frequency (MHz). (b) Deformation of the tissue-mimicking phantom (microns) containing microgels with 2% cross-linking versus stimulation frequency (MHz). (c) Deformation of the tissue-mimicking phantom (microns) containing microgels with 4% cross-linking versus stimulation frequency (MHz). (d) Deformation of the tissue-mimicking phantom (microns) containing microgels with 7% cross-linking versus stimulation frequency (MHz). Ten replications were run per condition. Error bars represent standard deviation. Mean values +/− standard deviation are presented

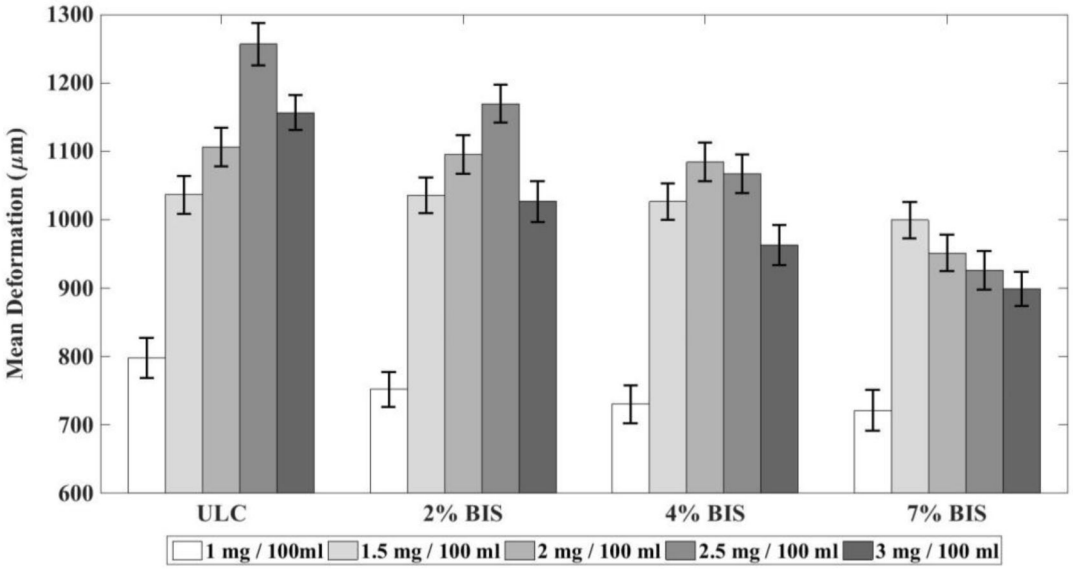

Figure 7.

Deformation of the tissue-mimicking phantom (microns) containing microgels under ultrasound stimulation of 1 MHz versus degree of cross-linking for (at various concentration.). Ten replications were run per condition. Error bars represent standard deviation. Mean values +/− standard deviation are presented.

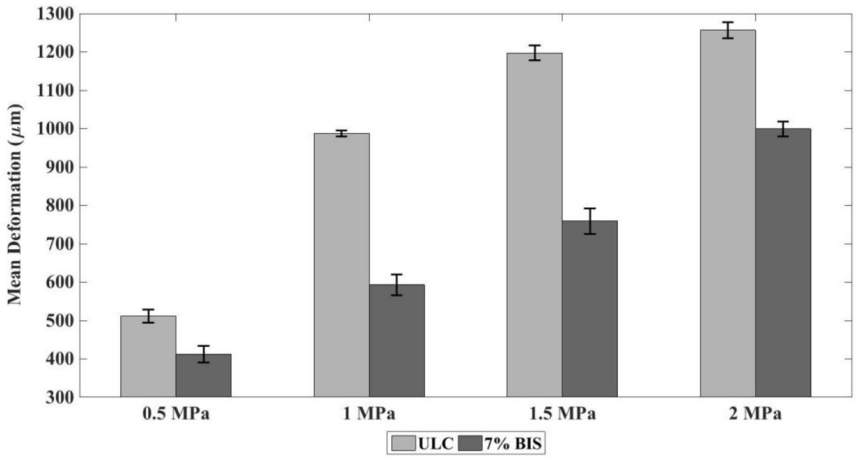

Figure 8.

Mean deformation of the tissue-mimicking phantom (microns) containing microgels with 0% cross-linking and 7 % cross-linking at a concentration of 2.5 mg / 100 ml of water and 1.5 mg / 100 ml of water respectively under ultrasound stimulation of 1 MHz versus peak-to-peak amplitude of ultrasound stimulation. Ten replications were run per condition. Error bars represent standard deviation. Mean values +/− standard deviation are presented

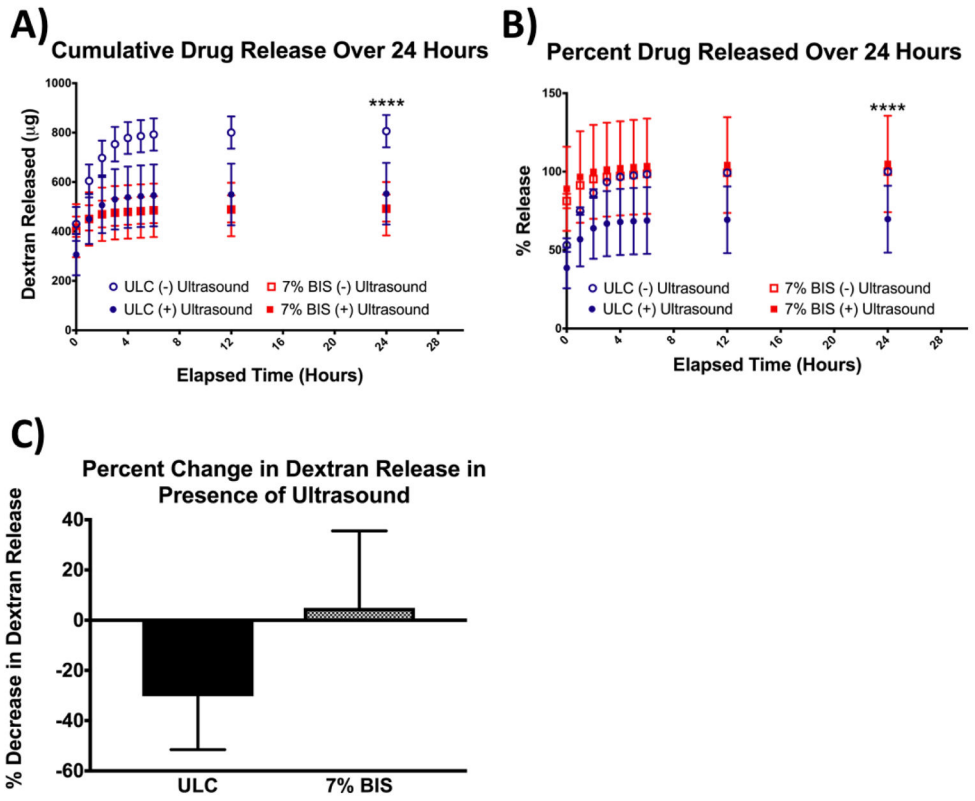

Figure 9.

(a) Cumulative release of 20 kDa dextran from ULC and 7% BIS microgels in the presence or absence of ultrasound. **(b)** Percent dextran released from ULC and 7% BIS microgels in the presence or absence of ultrasound, normalized to maximum release from each microgel type in the absence of ultrasound. **(c)** Percent change in cumulative dextran release after 24 hours from each microgel type in the presence of ultrasound. Error bars represent standard deviation from the mean.

Table 1

DLS measurements for various microgel compositions in formate buffer.[1]

Microgel	Diameter (nm)
ULC	764.0 ± 20.5
2% BIS	821.8 ± 47.0
4% BIS	760.3 ± 14.7
7% BIS	809.5 ± 164.6

[1]Microgels were suspended in 10 mM formate buffer (pH 3.0) in order to characterize sizes under acidic charge conditions. Due to the high degree of acrylic acid present within the microgels, the charges present in the formate buffer will cause the microgels to collapse. Four measurements of 13 runs each were performed on each microgel type in each buffer for a total of 52 runs per microgel type per buffer. Mean values ± standard deviation are presented.